Please cite this article in press as: Cueva et al., Posttranslational Acetylation of α-Tubulin Constrains Protofilament Number in Native Microtubules, Current Biology (2012), doi:10.1016/j.cub.2012.05.012

Current Biology 22, 1–9, June 19, 2012 ©2012 Elsevier Ltd All rights reserved DOI 10.1016/j.cub.2012.05.012

Article

Posttranslational Acetylation of α-Tubulin Constrains Protofilament Number in Native Microtubules

Juan G. Cueva,[1] Jen Hsin,[2] Kerwyn Casey Huang,[2] and Miriam B. Goodman[1,*]
[1]Department of Molecular and Cellular Physiology
[2]Department of Bioengineering
Stanford University, Stanford, CA 94305, USA

Summary

Background: Microtubules are built from linear polymers of α-β tubulin dimers (protofilaments) that form a tubular quinary structure. Microtubules assembled from purified tubulin in vitro contain between 10 and 16 protofilaments; however, such structural polymorphisms are not found in cells. This discrepancy implies that factors other than tubulin constrain microtubule protofilament number, but the nature of these constraints is unknown.

Results: Here, we show that acetylation of MEC-12 α-tubulin constrains protofilament number in *C. elegans* touch receptor neurons (TRNs). Whereas the sensory dendrite of wild-type TRNs is packed with a cross-linked bundle of long, 15-protofilament microtubules, *mec-17;atat-2* mutants lacking α-tubulin acetyltransferase activity have short microtubules, rampant lattice defects, and variable protofilament number both between and within microtubules. All-atom molecular dynamics simulations suggest a model in which acetylation of lysine 40 promotes the formation of interprotofilament salt bridges, stabilizing lateral interactions between protofilaments and constraining quinary structure to produce stable, structurally uniform microtubules in vivo.

Conclusions: Acetylation of α-tubulin is an essential constraint on protofilament number in vivo. We propose a structural model in which this posttranslational modification promotes the formation of lateral salt bridges that fine-tune the association between adjacent protofilaments and enable the formation of uniform microtubule populations in vivo.

Introduction

Microtubules have diverse functions and are needed for cell division, migration, and intracellular transport. They are fundamental elements of the eukaryotic cytoskeleton composed of linear polymers of α-β dimers (protofilaments) assembled into hollow tubes. It has been known for decades that the number of protofilaments that compose a microtubule varies significantly among cells [1, 2], despite a remarkable degree of tubulin sequence conservation both within and across species [3]. Such architectural polymorphisms are a pervasive feature of microtubules and are strikingly recapitulated among microtubules assembled in vitro from tissues that contain uniform microtubules [4]. This classic observation implies that lateral interactions between protofilaments are flexible enough to accommodate a wide range of bending angles and that factors present in cells constrain microtubule architecture and help to define the quinary structure of native microtubules.

*Correspondence: mbgoodman@stanford.edu

Complex, microtubule-based structures are a hallmark of many mechanoreceptor neurons, including the *C. elegans* touch receptor neurons (TRNs), which are low-threshold mechanoreceptor neurons. The TRNs are filled with dense, cross-linked arrays of as many as 50 15-protofilament (pf) microtubules [5]. Some cells in mammals [6, 7] and other invertebrates [8] also contain 15-pf microtubules. In *C. elegans* TRNs, these distinctive microtubules serve multiple functions, including the regulation of gene and protein expression [9], but are not essential for neurite outgrowth [10–12] or for activation of the mechanoelectrical transduction channels that initiate touch sensation [13, 14]. Not all *C. elegans* cells contain 15-pf microtubules [5], however. Thirteen-pf microtubules are found in sensory cilia, and 11-pf microtubules are the norm in most *C. elegans* cells, including other neurons [5]. Thus, different *C. elegans* cells form microtubules composed of 11, 13, or 15 protofilaments in a cell-specific manner.

The factors that regulate microtubule quinary structure and account for the well-known structural polymorphisms observed in vitro and in vivo have yet to be identified. One hypothesis is a tubulin code in which specific tubulin isoforms form specific microtubules [15]. Consistent with this idea, the TRNs coexpress *mec-7* β-tubulin and *mec-12* α-tubulin and depend on both tubulin genes to form large-diameter, 15-pf microtubules [10–12]. However, although MEC-7 and MEC-12 are expressed at high levels in TRNs, both are also expressed in neurons that lack 15-pf microtubules [12, 16]. Thus, although these tubulins are needed to form 15-pf microtubules, they may not be sufficient. Posttranslational modifications are another potential source of structural variation. Indeed, α-tubulin acetylation has been hypothesized to confer structural and thus functional heterogeneity to microtubules [17, 18], as it does to histones [19]. *C. elegans* expresses two α-tubulin acetyltransferases (α-TATs), *mec-17* and its paralog *atat-2* [20, 21], that catalyze acetylation of lysine 40 on α-tubulin. Both enzymes are expressed in TRNs [20, 21] where they acetylate MEC-12 α-tubulin, the sole K40-bearing α-tubulin in *C. elegans* [12]. The function of K40 acetylation, however, remains poorly understood.

Here, we combine genetic dissection, in vivo structure-function analysis, and serial-section, high-pressure freezing electron microscopy (EM) to demonstrate that α-tubulin K40 acetylation is needed to constrain microtubule pf number and quinary structure in TRNs in vivo. Based on all-atom molecular dynamics simulations, we propose a structural model in which α-tubulin K40 acetylation favors interprotofilament salt bridges and modulates lateral interactions in the microtubule lattice. This investigation is a vital first step toward a full definition of the factors that control the quinary structure of native microtubules in cells.

Results

We used serial-section EM of high-pressure-frozen animals to analyze microtubules with nanometer resolution [22] and to investigate how loss of α-TAT activity affects microtubule architecture. Individual 15-pf microtubules are approximately 20 μm long and organized in a staggered array that fills the

Please cite this article in press as: Cueva et al., Posttranslational Acetylation of α-Tubulin Constrains Protofilament Number in Native Microtubules, Current Biology (2012), doi:10.1016/j.cub.2012.05.012

Table 1. Microtubule Architecture in Wild-Type and α-TAT Mutants

Genotype	Transgene	n	MTs/ section	MT length (μm)[b]	pf number[c]
wild-type[a]	none	3	62 ± 7	20.1 ± 0.4	wild-type
mec-12	none	3	0 ± 0	0 ± 0	n/a
atat-2	none	3	37 ± 17	15 ± 2.4	wild-type
mec-17	none	3	8.8 ± 1.6	7.5 ± 2.8	variable
mec-17;atat-2	none	3	7.1 ± 0.6	2.29 ± 0.06	variable

n = the number of TRNs serially sectioned and examined for each genotype. Each serial section data set consisted of at least 60 ultrathin sections; individual sections were 50 nm thick.

[a]Data derived from an HPF-FS serial section data set reported in [22].

[b]Average microtubule length was calculated using the formula $L = 2Na/T$ where L is average microtubule length, N is the average number of microtubules per section, a is the length of the series, and T is the total number of microtubule terminations [5].

[c]Wild-type = most microtubules have 15 protofilaments, though rare 11-pf microtubules are present; variable = microtubules have 9 to 16 protofilaments.

entire neurite [5, 22], which is 500 μm long in wild-type (WT) adults. Microtubules in WT TRNs are heavily acetylated [23], as revealed by intense labeling with an antibody that specifically recognizes acetylated lysine 40 of α-tubulin (αK40Ac) [23, 24] and supported by the observation that both α-TATs are expressed in TRNs [20] and localize to the TRN cytoplasm (see Figure S1 available online). In *mec-12* null mutants, TRNs are devoid of 15-pf microtubules (Table 1; [14, 25]) and αK40Ac is undetectable [20, 21].

We counted the number of microtubules in our serial section data sets and used these counts to estimate the average microtubule length, as described previously [5]. Loss of α-TAT activity decreased both microtubule number and length (Table 1), suggesting that αK40Ac enables the formation and retention of long microtubules. Microtubules in WT TRNs are linked into a bundle by fine filaments [22]. Despite the decrease in microtubule number, intermicrotubule links were retained in α-TAT mutants: the average length of such links was 7.8 ± 2.0 nm (mean ± SD, n = 173) and 7.3 ± 1.9 nm (n = 185) in WT and *mec-17;atat-2* double mutants, respectively ($p = 0.02$, Student's t test). Taken together, these findings indicate that α-TAT enzymes and αK40 acetylation are needed to stabilize microtubule length and number and that the factors regulating individual microtubules are distinct from those organizing the bundle.

Disrupting the *mec-17* gene also diversified the number of protofilaments contained in each microtubule (Figures 1C and 1D). To examine this in detail, we developed a novel poststaining technique (see Experimental Procedures) and applied it to our high-pressure frozen, freeze-substituted (HPF-FS) samples. This technique allowed for direct visualization of microtubule protofilaments and provided resolution comparable to classical, tannic acid-based staining methods applied to thin sections. In agreement with previous studies [5, 22], the vast majority (>95%) of microtubules in WT TRNs have 15 protofilaments and the remainder have 11 protofilaments (Figure 1A). Microtubules in *atat-2* mutants also consisted primarily of 15-pf microtubules (Figure 1B), suggesting that the modest reduction in TRN αK40Ac levels associated with this mutant [20] does not affect protofilament number. In *mec-17* and *mec-17;atat-2* mutants where αK40Ac levels in TRNs are essentially undetectable [20], we found polymorphic microtubules consisting of as few as 10 and as many as 16 protofilaments (Figures 1C and 1D). Until now, such polymorphisms in microtubule quinary structure have only been observed in vitro [4, 26]. Thus, α-tubulin K40 acetylation is required to regulate protofilament number in vivo.

We observed differences in microtubule cross-section shape and area in all mutants. To quantify this variation, we developed a semiautomatic image processing workflow capable of measuring the area and eccentricity of microtubule profiles (see Experimental Procedures). Microtubule profiles were defined by finding a curve running approximately through the centers of the protofilaments; inner and outer circumferences were calculated from this curve assuming the microtubule formed an annulus of 6.5 nm thick protofilaments. Microtubule profiles in WT TRNs were essentially circular and had dimensions consistent with previous measurements of 15-pf microtubules in both fixed and frozen preparations [22, 27].

Microtubule size, but not shape, was similar in WT and *atat-2* animals (Figures 2A and 2C; Figure S2). We found an increase in the number of elliptical microtubule profiles in *atat-2* mutants (Figure 2C; Figure S2). To eliminate the possibility that such profiles arose from sectioning cylindrical profiles at oblique angles, we restricted our analysis to data sets in which the TRN plasma membrane could be resolved. We note that our analysis algorithm also excluded individual elliptical microtubule profiles that were not in sharp focus. This establishes that our thin sections are perpendicular to the long axis of the TRNs and the microtubule bundle. Both microtubule size and shape were variable in *mec-17* and *mec-17;atat-2* mutants (Figure 2; Figure S2). Narrowing our focus to the subset of large microtubules that retained 15 pfs in mutant TRNs revealed an increase in average eccentricity as well as an increase in the proportion of elliptical profiles (Figure 2E). Thus, partial loss of αK40 acetylation may weaken interprotofilament interactions and alter microtubule shape, whereas complete loss destabilizes quinary structure and enables the formation of microtubules with a variable number of protofilaments.

Based on the variations in microtubule shape, size, and protofilament number in α-TAT mutants (Figures 1 and 2), we propose that αK40Ac stabilizes interprotofilament interactions and the bending angle between protofilaments. To investigate the structural basis of the proposed effect of αK40 acetylation on lateral interactions between protofilaments, we generated a homology model of two neighboring MEC-12 α-tubulin monomers based on the work of Wells and Aksimentiev [28] (Figure S3A). This static model places αK40 close to αE55 in the H1′-S2 loop, suggesting that a salt bridge could form between these residues (Figure 3A). The model also reveals that αE55 could form a salt bridge with αH283 in the M-loop of the neighboring α-tubulin (Figure 3B), as suggested previously [29]. Upon lattice polymerization, αE55 could thus form a salt bridge either within a single α-tubulin monomer (with αK40) or between neighboring α-tubulins across the interprotofilament interface (with αH283). We propose a model in which acetylation of αK40 reduces the probability that αE55 forms an intramonomer salt bridge and increases the probability that it forms a salt bridge with the neighboring αH283 (Figure 3C). In this model (Figure 3D), αK40Ac strengthens lateral interactions between α-tubulins by promoting formation of interprotofilament salt bridges between adjacent α-tubulins. This loop-loop interaction is part of a flexible hinge that permits a wide range of interprotofilament angles required to accommodate different protofilament configurations [30–32].

We used all-atom molecular dynamics simulations to investigate the feasibility of this structural model. In these

Please cite this article in press as: Cueva et al., Posttranslational Acetylation of α-Tubulin Constrains Protofilament Number in Native Microtubules, Current Biology (2012), doi:10.1016/j.cub.2012.05.012

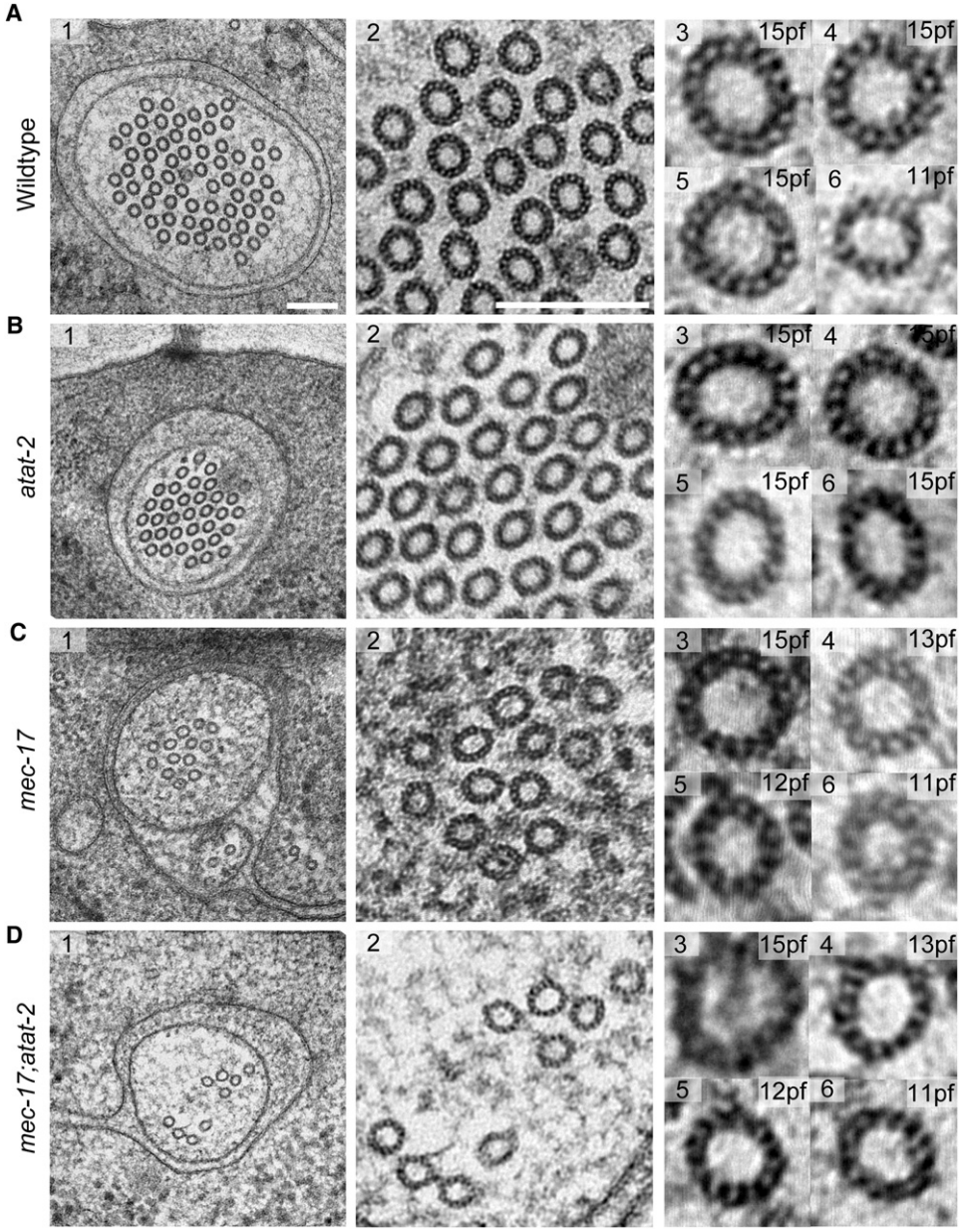

Figure 1. Alpha K40 Acetylation Is Required for the Formation of the Distinctive 15-pf Microtubules Present in TRNs and for Proper Cylindrical Shape

High-resolution electron micrographs of 50 nm thin sections of touch receptor neurons in WT (A), *atat-2(ok2415)* (B), *mec-17(ok2109)* (C), and *mec-17;atat-2* (D) animals. Scale bars represent 150 nm. See also Figure S1 for α-tubulin acetyltransferase expression pattern in TRNs.

simulations, we introduced a salt bridge for each pair of residues by bringing the two residues together with an external force. This force was gradually reduced to zero. A salt bridge was considered to be stable if the two residues remained in sufficient proximity to form a salt bridge after the force was released (Figure S3B). Using this strategy and this criterion for stability, we found that αE55 can form a stable intramonomer salt bridge with αK40 and a stable intermonomer salt bridge with αH283 (Movies S1 and S2). Following acetylation of αK40, only αE55 and αH283 maintained their electrostatic interaction (Movies S3 and S4), providing a structural substrate for interprotofilament stabilization. As a control, we also tested the stability of the intermonomer salt bridge between αE55 and αK280, because the latter residue is hypothesized to interact with αE90 [32]. As expected, αE55 and αK280 separated within 5 ns of the force being released, confirming that these two residues are unlikely to form a salt bridge (Figure S3B; Movies S5 and S6). Formation of the αE55-αH283 intermonomer salt bridge also increased the contact surface area between the MEC-12 subunits (Figure S3C), suggesting more stabilized interprotofilament interactions in the αK40-modified conformation.

To test whether acetylation of MEC-12[K40] could account for the observed effects on microtubule quinary structure, we used our HPF-FS technique to analyze microtubules in transgenic mutants expressing WT and mutant MEC-12 isoforms selectively in the touch receptor neurons [20]. As reported previously [14, 25], *mec-12* null mutants are devoid of

Please cite this article in press as: Cueva et al., Posttranslational Acetylation of α-Tubulin Constrains Protofilament Number in Native Microtubules, Current Biology (2012), doi:10.1016/j.cub.2012.05.012

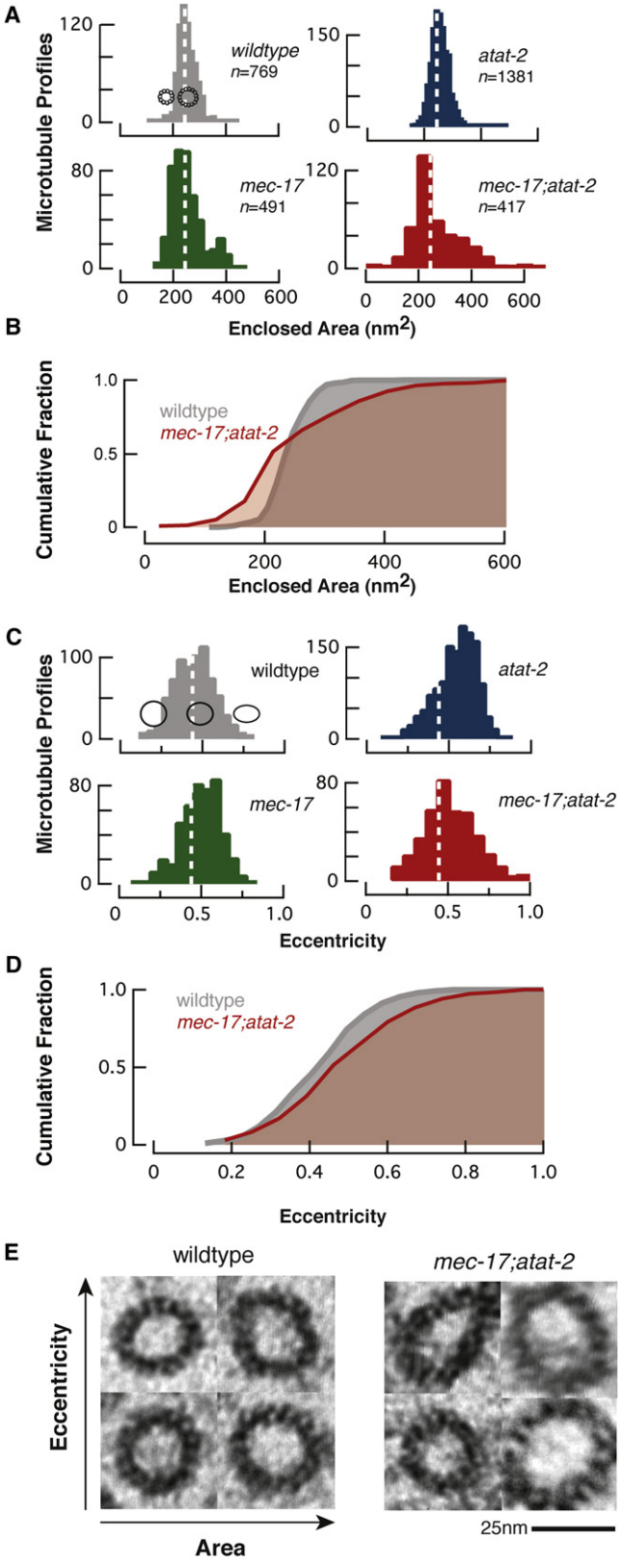

Figure 2. Loss of αK40Ac Alters the Size and Shape of TRN Microtubules

(A) Histograms showing the distribution of the area enclosed by microtubules in TRNs as a function of genotype. Dotted lines are at 244 nm^2, the mean area in WT TRNs. Schematics show 15-pf and 11-pf microtubules positioned along the x axis according to their predicted internal area.

15-pf microtubules (Table 1). Transgenic expression of MEC-12(+) allowed microtubules containing mostly 15 protofilaments to form in *mec-12* mutants (Figures 4A and 4D), but not in *mec-17;atat-2;mec-12* triple mutants (Figures 4B and 4D). Thus, transgenic expression of MEC-12(+) enables 15-pf microtubules to form only if the α-TAT genes, *mec-17* and *atat-2*, are intact. Despite the recapitulation of WT quinary structure in transgenic *mec-12*;MEC-12(+) animals, we observed significantly fewer microtubules in transgenic than in WT TRNs (Tables 1 and 2). The exact reason for this difference between intact and transgenic control TRNs is unclear, but a likely possibility is overexpression of UNC-86::MEC-3 binding sites in the *mec-17* promoter used to selectively express MEC-12 in the touch receptor neurons [20].

Reminiscent of the microtubule phenotype observed in α-TAT-deficient *mec-17;atat-2* double mutants, *mec-12* null mutant TRNs expressing MEC-12(K40R) harbored polymorphic microtubules (Figures 4C and 4D). Because this substitution replaces lysine 40 with a positively charged residue that cannot be acetylated [33], this finding suggests that the posttranslational modification per se is crucial for the formation or stability of 15-pf microtubules. The polymorphic microtubules in *mec-12* mutants expressing MEC-12(K40R) and in *mec-17;atat-2;mec-12* triple mutants expressing MEC-12(+) were similar in length and abundance. Both populations of polymorphic microtubules were approximately half as long and three times less abundant than the 15-pf microtubules found in *mec-12*;MEC-12(+) transgenic animals (Table 2). Collectively, these findings imply that α-tubulin acetylation is required to constrain microtubule quinary structure to 15-pf in TRNs.

Three-dimensional reconstructions of microtubules from serial sections of *mec-17* and *mec-17;atat-2* mutants revealed openings in the microtubule lattice (Figure 5) in half (18 out of 35) of the microtubules present in these mutants. Such openings have not been observed in >4,000 EM sections from over a dozen high-pressure frozen, freeze-substituted WT TRNs (data not shown). Although microtubule lattice openings have been reported in vitro [34, 35], to our knowledge, this is the first reported observation of microtubule lattice openings in vivo. Remarkably, many of these lattice openings extend for >150 nm, a length equivalent to nearly 20 tubulin dimers. Lattice defects were detected distal (~1 μm) to microtubule endpoints and were frequently associated with a change in protofilament number (Figure 5A). Thus, in the absence of α-tubulin acetyltransferase activity, microtubule lattice openings can occur in vivo and the lattice is sufficiently flexible to incorporate multiple quinary structures within a single microtubule. Future studies are needed to discern whether lattice openings and changes in protofilament number arise primarily

(B) Cumulative distribution functions comparing the size of WT and α-TAT-deficient *mec-17;atat-2* double mutants. α-TAT-deficient TRNs have an increase in smaller microtubules and a concomitant decrease in larger ones. The size distribution of mutant microtubules differs from WT ($p < 0.001$, Kolmogorov-Smirnov [KS] test).

(C) Histograms of microtubule eccentricity as a function of genotype. Dotted lines are at 0.44, the mean eccentricity for WT microtubules. Profiles show the shape of ellipses with eccentricity values of 0.25, 0.5, and 0.75.

(D) Cumulative distribution functions comparing the shape of WT and α-TAT-deficient *mec-17;atat-2* double mutants. α-TAT-deficient microtubules have more elliptical cross-sections.

(E) Fifteen-pf microtubules in WT (left) and α-TAT-deficient double mutants (right). Area increases from left to right; eccentricity increases from bottom to top. The scale bar applies to both panels. See also Figure S2.

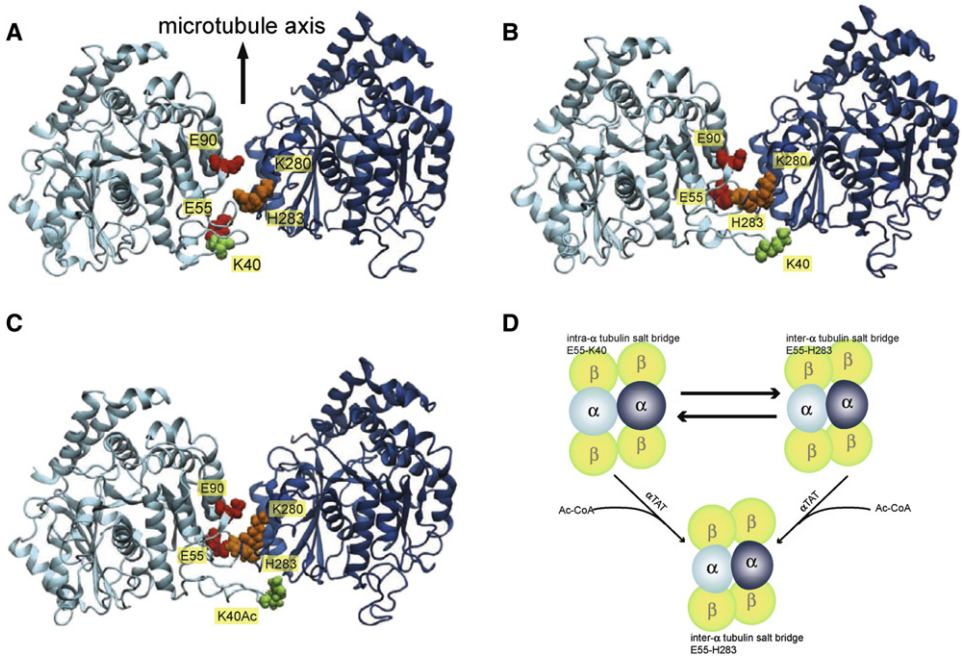

Figure 3. MEC-12 α-Tubulin Dimer Homology Model Incorporated into a Microtubule Lattice

Two adjacent MEC-12 monomers are colored in light and dark blue, and all views are from the luminal side of the interprotofilament interface. Key resides are shown in space-filling representation: αK40 (green), αE55 and αE90 (red), αK280 and αH283 (orange).

(A and B) αE55 can form an intramonomer salt bridge with αK40 (A) or an intermonomer salt bridge with H283 of the neighboring monomer (B).

(C) Following acetylation, αK40 can no longer form a salt bridge, and the intermonomer salt bridge between αE55 and αH283 is favored.

(D) Schematic of the proposed model for αK40 acetylation-mediated regulation of the protofilament lattice. See also Figure S3 and Movies S1, S2, S3, S4, S5, and S6 for salt bridge stability probed by molecular dynamics simulations.

from defects in polymerization, destabilization of lateral interactions between adjacent protofilaments, or a combination of both factors.

Discussion

Microtubules can contain fewer than 10 or as many as 16 protofilaments and are the target of numerous posttranslational modifications. We investigated the contribution of one posttranslational modification to microtubule architecture: the transfer of acetyl groups to lysine 40 of α-tubulin. This study leveraged two unique features of *C. elegans*: (1) MEC-12 α-tubulin is required to form bundles of distinctive, 15-pf microtubules in TRNs, and (2) of the 12 α-tubulins encoded by the *C. elegans* genome, MEC-12 is the only one with lysine at position 40. We report that disrupting the α-tubulin acetyltransferase genes *mec-17* and *atat-2* results in the formation of short, polymorphic microtubules in TRNs and that eliminating lysine 40 by mutating the residue to arginine likewise promotes the formation of short, polymorphic microtubules.

How might αK40Ac regulate protofilament number? Motivated by all-atom molecular dynamics simulations, we propose the following model: transfer of an acetyl group to αK40 disrupts an intramonomer salt bridge (αE55 to αK40) and favors a salt bridge between adjacent α-tubulin monomers (αE55 to αH283). The intermonomer salt bridge alters lateral interactions between α-tubulins, leading to interprotofilament angles consistent with 15-pf microtubules. In the absence of αK40Ac or if αK40 is replaced with arginine, αE55 might engage in either an intramonomer salt bridge (with αK40 or αR40) or an intermonomer salt bridge (with αH283) and, under these conditions, interprotofilament angle can assume a wider range of values, leading to elliptical microtubule profiles and variation in protofilament number both within and between microtubules. In principle, the lateral salt bridge could be formed at the interface between all α-tubulins, because most, if not all, isoforms have either a glutamate or aspartate at position 55 and a histidine at position 283.

To conclude, we have established that loss of α-tubulin K40 acetylation removes an essential in vivo constraint on microtubule architecture and used all-atom molecular dynamics simulations to develop a structural model of the mechanism of how enzymatic modification of a protein interface could alter quinary structure. However, because not all cells that coexpress α-TAT enzymes and K40-bearing α-tubulins form 15-protofilament microtubules, additional cell-specific factors that fine-tune interprotofilament angles and allow cells to count protofilaments remain to be discovered.

Experimental Procedures

Growth Conditions and Strains

Worms were raised on OP50 *E. coli*-seeded NGM plates at 20°C, following standard methods [36]. The following WT and mutant *C. elegans* strains were used: WT (N2), CB1607 *mec-12(e1607)* III, GN232 *mec-17(ok2109)* IV, GN233 *atat-2(ok2415)* X, GN234 *mec-17(ok2109)* IV; *atat-2(ok2415)* X, GN239 *mec-12(e1607)* III; *mec-17(ok2109)* IV; *atat-2(ok2415)* X. The following transgenic strains, derived as described previously [20], were used: GN280 *mec-12(e1607)* III; *pgEx46*(*P*mec-17::MEC-12[+], *P*unc-122::RFP), GN283 *mec-12(e1607)* III; *pgEx49*(*P*mec-17::MEC-12[K40R], *P*unc-122::RFP), GN295 *mec-12(e1607)* III; *mec-17(ok2109)* IV; *atat-2(ok2415)* X; *pgEx58*(*P*mec-17::MEC-12[+], *P*unc-122::RFP).

Serial-Section Electron Microscopy

Adult nematodes were prepared for EM as previously described [22]. Briefly, animals were frozen using an EMPACT2 high-pressure freezer system

Please cite this article in press as: Cueva et al., Posttranslational Acetylation of α-Tubulin Constrains Protofilament Number in Native Microtubules, Current Biology (2012), doi:10.1016/j.cub.2012.05.012

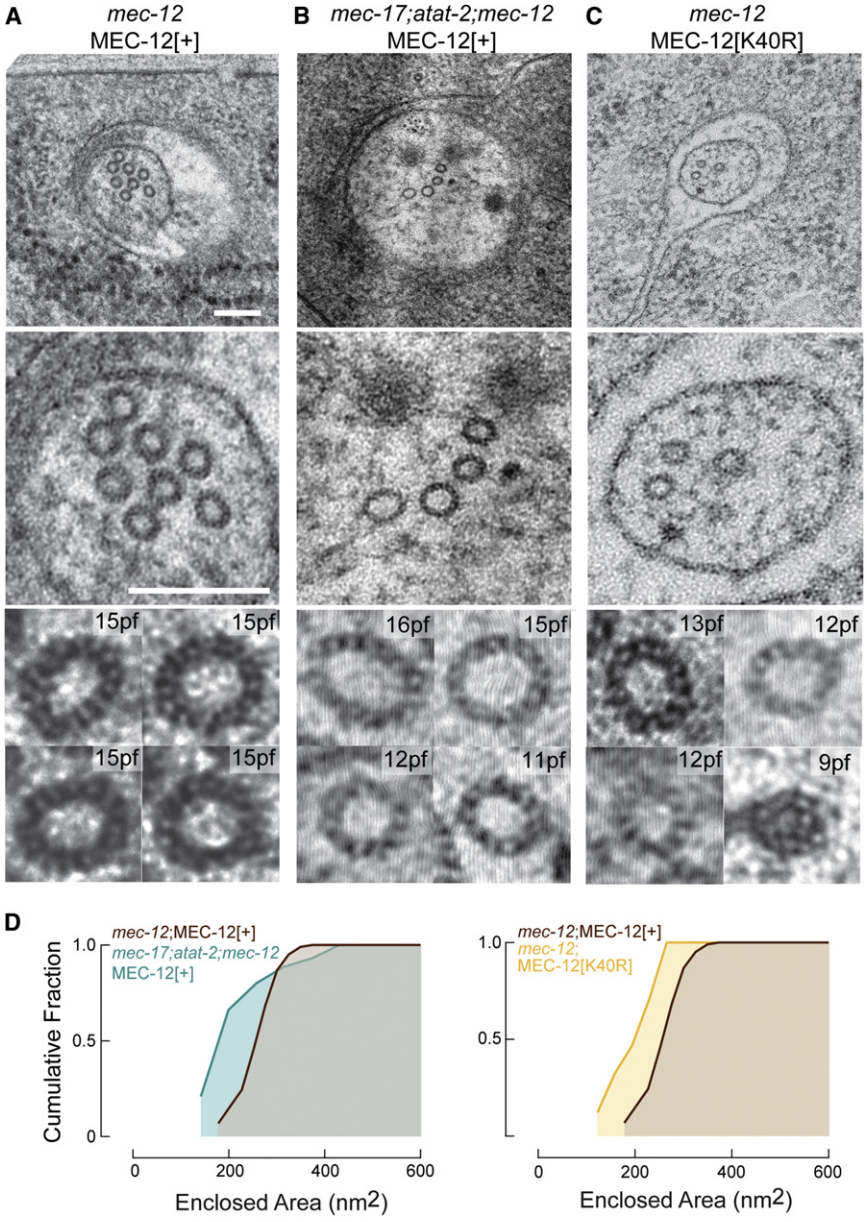

Figure 4. Loss of α-TAT Genes or αK40 Diversifies Microtubule Quinary Structure

(A) Transgenic expression of MEC-12(+) in *mec-12(e1607)* null mutants restores essentially uniform 15-pf quinary structure. Scale bars represent 150 nm and apply to (A), (B), and (C).

(B) Transgenic expression of MEC-12(+) in *mec-17;atat-2;mec-12* triple mutants results in polymorphic TRN microtubules.

(C) Transgenic MEC-12(K40R) induces polymorphic TRN microtubules in *mec-12* mutants.

(D) Cumulative distribution function of microtubule size in transgenic TRNs. Measurements obtained from 3–5 serial-section data sets. The size distribution of *mec-17;atat-2;mec-12;*MEC-12(+) (n = 115) and *mec-12;*MEC-12(K40R) (n = 90) differ significantly from *mec-12;*MEC-12(+) (n = 205) ($p < 0.001$, KS test).

(Leica, Vienna, Austria). A Leica AFS freeze substitution apparatus was used to preserve and embed nematodes in 2% glutaraldehyde plus 1% osmium tetroxide and in Eponate 12/Araldite 502. Serial, ultrathin (50 nm) sections were cut with a diamond knife on a Leica Ultracut S microtome and collected on Formvar-coated copper-slot grids. To enhance contrast, we poststained sections in 3.5% uranyl acetate (30 s) and Reynold's lead citrate preparation (3 min). The grids were imaged on a transmission electron microscope (JEOL TEM 1230, Tokyo, Japan), and images were acquired with an 11 megapixel bottom-mounted cooled CCD camera (Orius SC1000, Gatan, Pleasanton, CA). Three-dimensional models were generated from serial sections with Reconstruct [37]. Images of consecutive sections were aligned manually.

Computational Determination of Microtubule Geometries

Segmentation proceeded in two steps: first, approximate outlines of the microtubules were identified; second, the outlines were refined based on local intensity distributions to accurately quantify area, perimeter, and eccentricity. EM images were filtered to smooth variations at length scales larger than a typical microtubule and to attenuate structures smaller than the width of a protofilament. Each image was then contrast-adjusted and a Gaussian filter was applied to smooth the image and remove pixel-to-pixel variation. All further operations were performed on the negative of the image so that the microtubules appeared as bright regions. The background was subtracted using morphological opening with a disk element of a similar size to the protofilament width, and the image was thresholded to create a binary image. Objects in the binary image were then thinned to lines and spur pixels were removed until no further changes occurred. The remaining closed curves were filtered based on size to identify microtubules. Microtubules that exhibited significant bending within the section appeared blurred and hence were ignored. All image processing was performed in Matlab (The Mathworks, Natick, MA).

The eccentricity of microtubules was calculated to provide a measure of the noncircularity of microtubules. The eccentricity of an ellipse is defined as $(1 - r^2_{minor}/r^2_{major})^{1/2}$, where r_{minor} and r_{major} are the minor and major axes, respectively. The eccentricity is invariant upon uniform scaling of the shape and is bounded by 0 (a circle) and 1 (a line).

Homology Model Construction and Molecular Dynamics Simulations

The atomic model of *C. elegans* MEC-12 was constructed based on a previous model of *B. taurus* α-tubulin dimer [28]. This *B. taurus* α-tubulin dimer model incorporated available crystallographic structures [30, 38, 39], as well as the structural information in a cryo-EM map of a microtubule at 8 Å resolution [32]. The *B. taurus* α-tubulin and *C. elegans* MEC-12 share more than 90% sequence identity, therefore homology modeling was straightforward. After the necessary mutations were introduced in the *B. taurus* α-tubulin dimer model [28] to transform it into a *C. elegans* MEC-12 dimer model, energy minimization was performed for 5,000 steps with the molecular dynamics package NAMD [40] to avoid clashes between side chains. Construction of the homology model was performed with the molecular rendering software VMD [41]. All molecular dynamics simulations were performed using NAMD [40] with protein and ion molecules described by the CHARMM27 force field with CMAP corrections [42–44] and water molecules described with the TIP3P model [45]. Standard simulation parameters were used [40].

In each simulation, an external force was used to bring the two residues into proximity and was gradually reduced to zero at 4.5 ns, followed by nearly 5 ns of simulation in the absence of any force to determine whether the amino acid pair maintained its interaction. To reduce the degrees of freedom of the simulated systems, we constrained most protein Cα atoms except the following amino acids: residues 35 to 60 (residing in the flexible H1′-S2 loop and not resolved in crystal structure [30, 38]) and residues 272

Please cite this article in press as: Cueva et al., Posttranslational Acetylation of α-Tubulin Constrains Protofilament Number in Native Microtubules, Current Biology (2012), doi:10.1016/j.cub.2012.05.012

Table 2. Microtubule Architecture Depends on the Acetylation State of MEC-12 αK40

Genotype	Transgene	n	MTs/ section	MT length (μm)[a]	pf number[b]
mec-12	MEC-12(+)	3	6.0 ± 0.7	14.7 ± 0.7	wild-type
mec-12;mec-17; atat-2	MEC-12(+)	3	3.0 ± 0.7	7.9 ± 1.6	variable
mec-12	MEC-12(K40R)	5	2.2 ± 1.0	6.8 ± 3.4	variable

n = the number of TRNs serially sectioned and examined for each genotype. Each data set consisted of at least 60 ultrathin (50 nm) serial sections.
[a]Average microtubule length was calculated using the formula $L = 2Na/T$ where L is average microtubule length, N is the average number of microtubules per section, a is the length of the series, and T is the total number of microtubule terminations [5].
[b]Wild-type = most microtubules have 15 protofilaments, though rare 11-pf microtubules are present; variable = microtubules have 9 to 16 protofilaments.

to 287 (residing in the M-loop, which required structural modification to match an EM density [46]). Molecular trajectories of the simulations are included as movies in Supplemental Information.

Supplemental Information

Supplemental Information includes three figures and six movies and can be found with this article online at doi:10.1016/j.cub.2012.05.012.

Acknowledgments

We thank C. Gao for worm injection, S. Watanabe and E. Jorgensen (University of Utah) for high-pressure freezing some samples while Stanford's equipment was being repaired, the Stanford Cell Sciences Imaging Facility for their EM facility, and M. Chalfie and the Caenorhabditis Genetics Center for strains. Work was supported by National Institutes of Health grants RO1NS047715 (M.B.G.), RO1EB006745 (M.B.G.), and DP2OD006466 (K.C.H.), National Science Foundation (NSF) grant EF1038697 (K.C.H.), and a Stanford University School of Medicine Dean's Postdoctoral Fellowship (J.H.). Molecular dynamics simulations were performed using the Extreme Science and Engineering Discovery Environment (XSEDE), supported by the NSF OCI-1053575, under allocation number TG-MCB110056 (J.H. and K.C.H.).

Received: February 20, 2012
Revised: April 24, 2012
Accepted: May 8, 2012
Published online: May 31, 2012

References

1. Burton, P.R., Hinkley, R.E., and Pierson, G.B. (1975). Tannic acid-stained microtubules with 12, 13, and 15 protofilaments. J. Cell Biol. *65*, 227–233.
2. Tilney, L.G., Bryan, J., Bush, D.J., Fujiwara, K., Mooseker, M.S., Murphy, D.B., and Snyder, D.H. (1973). Microtubules: evidence for 13 protofilaments. J. Cell Biol. *59*, 267–275.
3. McKean, P.G., Vaughan, S., and Gull, K. (2001). The extended tubulin superfamily. J. Cell Sci. *114*, 2723–2733.
4. Pierson, G.B., Burton, P.R., and Himes, R.H. (1978). Alterations in number of protofilaments in microtubules assembled in vitro. J. Cell Biol. *76*, 223–228.
5. Chalfie, M., and Thomson, J.N. (1979). Organization of neuronal microtubules in the nematode *Caenorhabditis elegans*. J. Cell Biol. *82*, 278–289.
6. Saito, K., and Hama, K. (1982). Structural diversity of microtubules in the supporting cells of the sensory epithelium of guinea pig organ of Corti. J. Electron Microsc. (Tokyo) *31*, 278–281.
7. Kikuchi, T., Takasaka, T., Tonosaki, A., Watanabe, H., Hozawa, K., Shinkawa, H., and Wada, H. (1991). Microtubule subunits of guinea pig vestibular epithelial cells. Acta Otolaryngol. Suppl. *481*, 107–111.
8. Mogensen, M.M., and Tucker, J.B. (1987). Evidence for microtubule nucleation at plasma membrane-associated sites in Drosophila. J. Cell Sci. *88*, 95–107.
9. Bounoutas, A., Kratz, J., Emtage, L., Ma, C., Nguyen, K.C., and Chalfie, M. (2011). Microtubule depolymerization in *Caenorhabditis elegans* touch receptor neurons reduces gene expression through a p38 MAPK pathway. Proc. Natl. Acad. Sci. USA *108*, 3982–3987.
10. Chalfie, M., and Sulston, J. (1981). Developmental genetics of the mechanosensory neurons of *Caenorhabditis elegans*. Dev. Biol. *82*, 358–370.
11. Savage, C., Hamelin, M., Culotti, J.G., Coulson, A., Albertson, D.G., and Chalfie, M. (1989). *mec-7* is a beta-tubulin gene required for the production of 15-protofilament microtubules in *Caenorhabditis elegans*. Genes Dev. *3*, 870–881.
12. Fukushige, T., Siddiqui, Z.K., Chou, M., Culotti, J.G., Gogonea, C.B., Siddiqui, S.S., and Hamelin, M. (1999). MEC-12, an alpha-tubulin required for touch sensitivity in *C. elegans*. J. Cell Sci. *112*, 395–403.
13. O'Hagan, R., Chalfie, M., and Goodman, M.B. (2005). The MEC-4 DEG/ENaC channel of *Caenorhabditis elegans* touch receptor neurons transduces mechanical signals. Nat. Neurosci. *8*, 43–50.
14. Bounoutas, A., O'Hagan, R., and Chalfie, M. (2009). The multipurpose 15-protofilament microtubules in *C. elegans* have specific roles in mechanosensation. Curr. Biol. *19*, 1362–1367.
15. Wade, R.H. (2009). On and around microtubules: an overview. Mol. Biotechnol. *43*, 177–191.
16. Hamelin, M., Scott, I.M., Way, J.C., and Culotti, J.G. (1992). The *mec-7* beta-tubulin gene of *Caenorhabditis elegans* is expressed primarily in the touch receptor neurons. EMBO J. *11*, 2885–2893.
17. Verhey, K.J., and Gaertig, J. (2007). The tubulin code. Cell Cycle *6*, 2152–2160.
18. Janke, C., and Kneussel, M. (2010). Tubulin post-translational modifications: encoding functions on the neuronal microtubule cytoskeleton. Trends Neurosci. *33*, 362–372.
19. Lee, J.-S., Smith, E., and Shilatifard, A. (2010). The language of histone crosstalk. Cell *142*, 682–685.
20. Shida, T., Cueva, J.G., Xu, Z., Goodman, M.B., and Nachury, M.V. (2010). The major alpha-tubulin K40 acetyltransferase alphaTAT1 promotes rapid ciliogenesis and efficient mechanosensation. Proc. Natl. Acad. Sci. USA *107*, 21517–21522.
21. Akella, J.S., Wloga, D., Kim, J., Starostina, N.G., Lyons-Abbott, S., Morrissette, N.S., Dougan, S.T., Kipreos, E.T., and Gaertig, J. (2010). MEC-17 is an α-tubulin acetyltransferase. Nature *467*, 218–222.
22. Cueva, J.G., Mulholland, A., and Goodman, M.B. (2007). Nanoscale organization of the MEC-4 DEG/ENaC sensory mechanotransduction channel in *Caenorhabditis elegans* touch receptor neurons. J. Neurosci. *27*, 14089–14098.
23. Siddiqui, S.S., Aamodt, E., Rastinejad, F., and Culotti, J. (1989). Anti-tubulin monoclonal antibodies that bind to specific neurons in *Caenorhabditis elegans*. J. Neurosci. *9*, 2963–2972.
24. Piperno, G., and Fuller, M.T. (1985). Monoclonal antibodies specific for an acetylated form of alpha-tubulin recognize the antigen in cilia and flagella from a variety of organisms. J. Cell Biol. *101*, 2085–2094.
25. Chalfie, M., and Au, M. (1989). Genetic control of differentiation of the *Caenorhabditis elegans* touch receptor neurons. Science *243*, 1027–1033.
26. Unger, E., Böhm, K.J., and Vater, W. (1990). Structural diversity and dynamics of microtubules and polymorphic tubulin assemblies. Electron Microsc. Rev. *3*, 355–395.
27. Chalfie, M., and Thomson, J.N. (1982). Structural and functional diversity in the neuronal microtubules of *Caenorhabditis elegans*. J. Cell Biol. *93*, 15–23.
28. Wells, D.B., and Aksimentiev, A. (2010). Mechanical properties of a complete microtubule revealed through molecular dynamics simulation. Biophys. J. *99*, 629–637.
29. Li, H., DeRosier, D.J., Nicholson, W.V., Nogales, E., and Downing, K.H. (2002). Microtubule structure at 8 A resolution. Structure *10*, 1317–1328.
30. Löwe, J., Li, H., Downing, K.H., and Nogales, E. (2001). Refined structure of alpha beta-tubulin at 3.5 A resolution. J. Mol. Biol. *313*, 1045–1057.
31. Nogales, E., Whittaker, M., Milligan, R.A., and Downing, K.H. (1999). High-resolution model of the microtubule. Cell *96*, 79–88.
32. Sui, H., and Downing, K.H. (2010). Structural basis of interprotofilament interaction and lateral deformation of microtubules. Structure *18*, 1022–1031.

Please cite this article in press as: Cueva et al., Posttranslational Acetylation of α-Tubulin Constrains Protofilament Number in Native Microtubules, Current Biology (2012), doi:10.1016/j.cub.2012.05.012

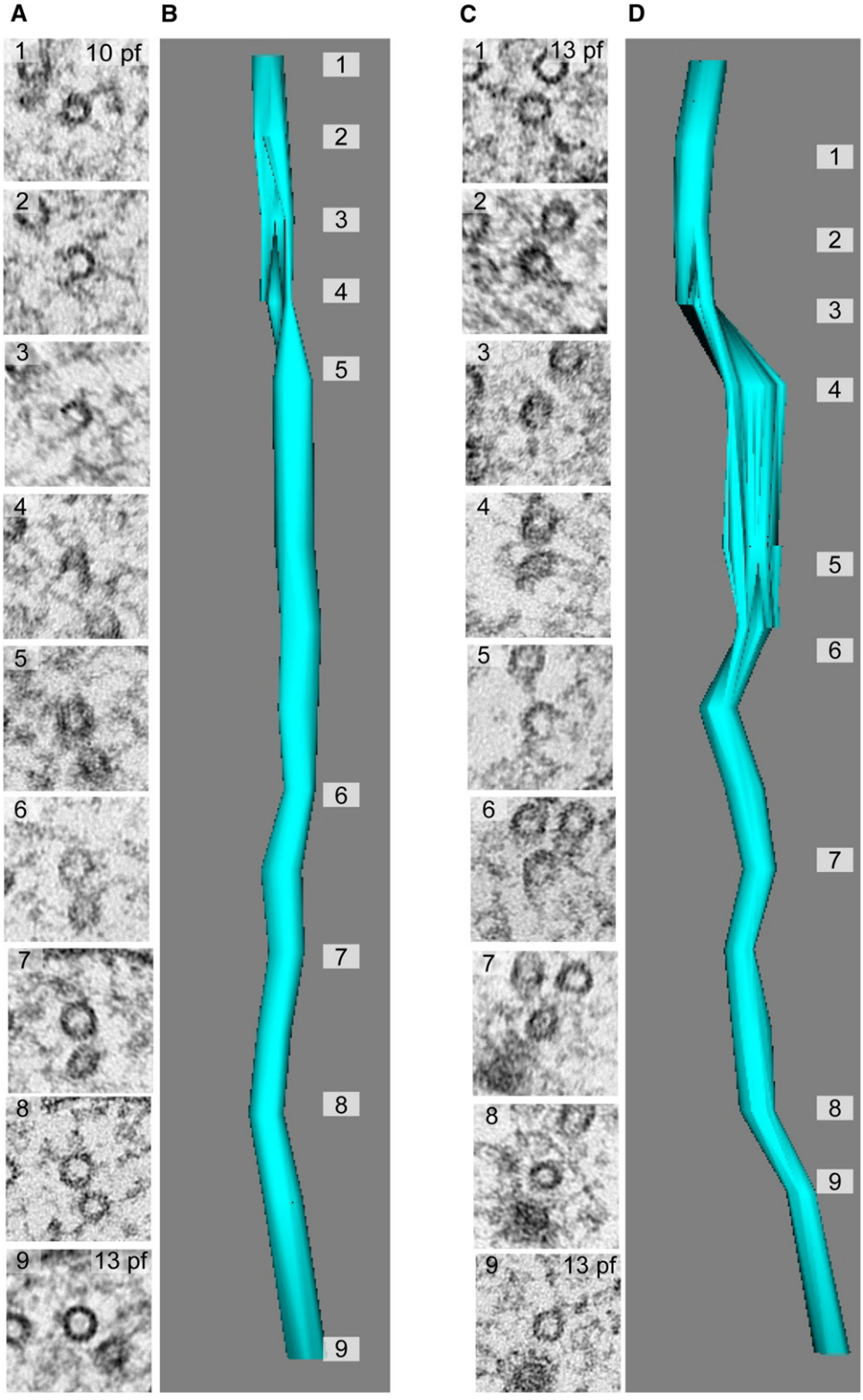

Figure 5. Loss of α-TAT Activity Reveals Lattice Defects and Variations in Protofilament Number in Individual Microtubules

(A and B) Example of a microtubule lattice defect associated with a change in protofilament number on opposite sides of the defect (10 versus 13).
(C and D) Example of a microtubule lattice defect with no change in protofilament number. Images were selected from two serial-section reconstructions consisting of 17 consecutive thin (50 nm) sections. The data sets were used to reconstruct two TRN microtubules in *mec-17;atat-2* double mutants.

Please cite this article in press as: Cueva et al., Posttranslational Acetylation of α-Tubulin Constrains Protofilament Number in Native Microtubules, Current Biology (2012), doi:10.1016/j.cub.2012.05.012

33. Gaertig, J., Cruz, M.A., Bowen, J., Gu, L., Pennock, D.G., and Gorovsky, M.A. (1995). Acetylation of lysine 40 in alpha-tubulin is not essential in *Tetrahymena thermophila*. J. Cell Biol. *129*, 1301–1310.
34. Chrétien, D., Metoz, F., Verde, F., Karsenti, E., and Wade, R.H. (1992). Lattice defects in microtubules: protofilament numbers vary within individual microtubules. J. Cell Biol. *117*, 1031–1040.
35. Chrétien, D., and Fuller, S.D. (2000). Microtubules switch occasionally into unfavorable configurations during elongation. J. Mol. Biol. *298*, 663–676.
36. Stiernagle, T. (2006). Maintenance of *C. elegans*. WormBook, 1–11. 10.1895/wormbook.1.101.1.
37. Fiala, J.C. (2005). Reconstruct: a free editor for serial section microscopy. J. Microsc. *218*, 52–61.
38. Nogales, E., Wolf, S.G., and Downing, K.H. (1998). Structure of the alpha beta tubulin dimer by electron crystallography. Nature *391*, 199–203.
39. Ravelli, R.B.G., Gigant, B., Curmi, P.A., Jourdain, I., Lachkar, S., Sobel, A., and Knossow, M. (2004). Insight into tubulin regulation from a complex with colchicine and a stathmin-like domain. Nature *428*, 198–202.
40. Phillips, J.C., Braun, R., Wang, W., Gumbart, J., Tajkhorshid, E., Villa, E., Chipot, C., Skeel, R.D., Kalé, L., and Schulten, K. (2005). Scalable molecular dynamics with NAMD. J. Comput. Chem. *26*, 1781–1802.
41. Humphrey, W., Dalke, A., and Schulten, K. (1996). VMD: visual molecular dynamics. J Mol Graph *14*, 33–38.
42. MacKerell, A.D., Bashford, D., Bellott, M., Dunbrack, R.L., Evanseck, J.D., Field, M.J., Fischer, S., Gao, J., Guo, H., Ha, S., et al. (1998). All-atom empirical potential for molecular modeling and dynamics studies of proteins. J. Phys. Chem. B *102*, 3586–3616.
43. Foloppe, N., and MacKerell, A.D., Jr. (2000). All-atom empirical force field for nucleic acids: I. Parameter optimization based on small molecule and condensed phase macromolecular target data. J. Comput. Chem. *21*, 86–104.
44. MacKerell, A.D., Jr., Feig, M., and Brooks, C.L., 3rd. (2004). Extending the treatment of backbone energetics in protein force fields: limitations of gas-phase quantum mechanics in reproducing protein conformational distributions in molecular dynamics simulations. J. Comput. Chem. *25*, 1400–1415.
45. Jorgensen, W.L., Chandrasekhar, J., Madura, J.D., Impey, R.W., and Klein, M.L. (1983). Comparison of simple potential functions for simulating liquid water. J. Chem. Phys. *79*, 926–935.
46. Sui, H., and Downing, K.H. (2006). Molecular architecture of axonemal microtubule doublets revealed by cryo-electron tomography. Nature *442*, 475–478.